




## Quasiuniversality from all-in–all-out Weyl quantum criticality in pyrochlore iridates

David J. Moser  and Lukas Janssen *Institut für Theoretische Physik and Würzburg-Dresden Cluster of Excellence ct.qmat, TU Dresden, 01062 Dresden, Germany* (Received 17 May 2023; revised 26 January 2024; accepted 29 January 2024; published 20 February 2024)

We identify an exotic quasiuniversal behavior near the all-in–all-out Weyl quantum critical point in three-dimensional Luttinger semimetals, such as the pyrochlore iridates  $R_2\text{Ir}_2\text{O}_7$ , with  $R$  a rare-earth element. The quasiuniversal behavior is characterized by power laws with exponents that vary slowly over several orders of magnitude in energy or length. However, in contrast to the quasiuniversality discussed in the context of deconfined criticality, the present case is characterized by a genuinely universal ultra-low-temperature behavior. In this limit, the pertinent critical exponents can be computed exactly within a renormalization group analysis. Experimental implications for the pyrochlore iridates are outlined.

DOI: [10.1103/PhysRevB.109.L081111](https://doi.org/10.1103/PhysRevB.109.L081111)

Quasiuniversality refers to a situation in which observables display apparent critical behavior over several orders of magnitude of energy or length, where, however, closer inspections of the observed power laws reveal slow drifts in the corresponding exponents [1–3]. Such a situation has recently been intensely discussed in the context of deconfined quantum criticality between antiferromagnetic and valence-bond-solid orders in two-dimensional quantum magnets [4,5]. In this case, the quasiuniversal behavior observed in numerical simulations [6] is believed to arise from a collision and subsequent annihilation of the corresponding critical fixed point with another, bicritical, fixed point, leaving behind a slow renormalization group flow [1–3,7]. In this scenario, the ultra-low-temperature behavior is ultimately weakly first order, with, however, a large finite-temperature regime characterized by quasiuniversality. An alternative interpretation of the numerical data is the presence of a second divergent length scale at criticality [8]. In this competing scenario, the low-temperature behavior is genuinely universal, but requires an adapted scaling ansatz accommodating the presence of the additional length scale.

In the present Letter, we identify quasiuniversal behavior in a three-dimensional model relevant to a class of pyrochlore iridates with chemical composition  $R_2\text{Ir}_2\text{O}_7$ , where  $R$  is a rare-earth element, e.g.,  $R = \text{Pr}, \text{Nd}$ . In their metallic phases, these compounds exhibit an electronic excitation spectrum characterized by quadratic band touching at the Fermi level [9,10], and as such fall into the larger class of Luttinger semimetals [11,12]. However, in comparison with the prominent members of this class,  $\text{HgTe}$  [13] and  $\alpha\text{-Sn}$  [14], the pyrochlore iridates feature a substantially increased effective quasiparticle mass, implying an enhanced role of electronic interactions [15,16]. If strong enough, these interactions can drive symmetry-breaking transitions, across which the electronic spectrum becomes partially or fully gapped out. Many pyrochlore iridates, such as  $\text{Nd}_2\text{Ir}_2\text{O}_7$  [10,17], indeed display a finite-temperature transition, below which the iridium moments feature all-in–all-out (AIAO) antiferromagnetic order. This state breaks time reversal but preserves crystal symmetries [18].  $\text{Pr}_2\text{Ir}_2\text{O}_7$ , by contrast, appears to remain disordered

up to the lowest accessible temperatures [15,19]. By varying the concentration  $x$  in  $(\text{Pr}_x\text{Nd}_{1-x})_2\text{Ir}_2\text{O}_7$  and/or by applying hydrostatic pressure, the Néel temperature associated with the onset of AIAO order can be tuned to zero, uncovering an underlying quantum phase transition [20]. Small AIAO order converts the quadratic band touching point into eight symmetry-related linear band crossing points [21–23]. Consequently, the quantum phase transition is expected to separate the symmetric Luttinger semimetal from a time-reversal-broken Weyl semimetal. The presence of gapless fermions at the transition indicates the possibility of unconventional behavior. In fact, previous theoretical work suggested a novel type of fermionic quantum critical point [24,25]. Here, we elucidate the finite-temperature properties of this transition, relevant for the experiments on the pyrochlore iridates. We reveal a large finite-temperature regime above the quantum critical point that is characterized by quasiuniversality (see Fig. 1). This unusual behavior arises from the presence of a marginally irrelevant coupling at the corresponding renormalization group fixed point. Importantly, we present an approach that allows us to identify properties of this fermionic quantum critical point exactly, including its nontrivial critical exponents. Our results reveal the AIAO Weyl quantum critical point in pyrochlore iridates as a unique instance of an interacting continuous quantum phase transition that is both experimentally and theoretically accessible. As a side product, we demonstrate the emergence of strong cubic anisotropy at criticality, thereby resolving an apparent contradiction in the literature [24,25].

*Model.* At the quantum critical point, the system can be effectively described by a continuum Euclidean action  $S = \int d\tau d^3x L$ , with Lagrangian  $L = L_0 + L_a + L_\phi$ . Here,  $L_0$  describes noninteracting electronic quasiparticles near the quadratic band touching [26–31],

$$L_0 = \sum_{i=1}^N \psi_i^\dagger \left( \partial_\tau + \sum_{a=1}^5 (1 + s_a \delta) d_a (-i\nabla) \gamma_a \right) \psi_i, \quad (1)$$

and originates in the Luttinger Hamiltonian [32]. In the above,  $N$  corresponds to the number of band touching points

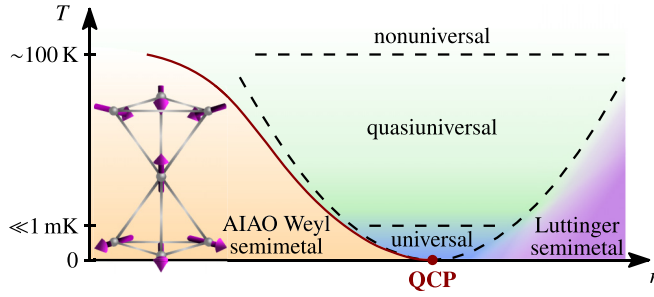


FIG. 1. Schematic finite-temperature phase diagram of pyrochlore iridates  $R_2\text{Ir}_2\text{O}_7$  near the quantum critical point (QCP) between the Weyl semimetal with all-in-all-out (AIAO) order, sketched in the inset, and the symmetric Luttinger semimetal.  $r$  indicates a nonthermal tuning parameter, such as chemical doping or hydrostatic pressure. Between the nonuniversal high-temperature regime and the genuinely universal ultra-low-temperature regime, there is a large quasiuniversal regime, characterized by power laws with slowly varying exponents.

at the Fermi level, with  $N = 1$  in the case of the pyrochlore iridates,  $\psi_i$  is a four-component Grassmann field,  $s_a := 1$  ( $s_a := -1$ ) for  $a = 1, 2, 3$  ( $a = 4, 5$ ),  $\delta$  parametrizes the cubic anisotropy with  $-1 \leq \delta \leq 1$ , the  $4 \times 4$  matrices  $\gamma_a$  fulfill the Euclidean Clifford algebra,  $\{\gamma_a, \gamma_b\} = 2\delta_{ab}\mathbb{1}$ , and  $d_a$  are proportional to  $\ell = 2$  real spherical harmonics, viz.,  $d_1(\vec{p}) = \sqrt{3}p_y p_z$ ,  $d_2(\vec{p}) = \sqrt{3}p_x p_z$ ,  $d_3(\vec{p}) = \sqrt{3}p_x p_y$ ,  $d_4(\vec{p}) = \frac{\sqrt{3}}{2}(p_x^2 - p_y^2)$ , and  $d_5(\vec{p}) = \frac{1}{2}(2p_z^2 - p_x^2 - p_y^2)$ . Moreover, we account for the long-range Coulomb interaction  $\sim 1/|\vec{x}|$  via [29,33,34]

$$L_a = \frac{1}{2}(\nabla a)^2 + iea \sum_{i=1}^N \psi_i^\dagger \psi_i, \quad (2)$$

where  $a$  denotes the scalar Coulomb field, and  $e$  the effective charge. Fluctuations corresponding to AIAO ordering on the pyrochlore lattice are parametrized by an Ising field  $\phi$ , and couple to the electronic quasiparticles as [24,25,35]

$$L_\phi = \frac{1}{2}\phi(r - \nabla^2)\phi + g\phi \sum_{i=1}^N \psi_i^\dagger \gamma_{45} \psi_i. \quad (3)$$

Here,  $r$  denotes the tuning parameter for the quantum phase transition,  $g$  the coupling constant, and  $\gamma_{45} := i\gamma_4\gamma_5$ . A term  $(\partial_\tau \phi)^2$  can be included in Eq. (3) as well, but is power-counting irrelevant and as such does not change the critical behavior. The same is true for bosonic self-interactions, such as a  $\phi^4$  term. A finite expectation value  $\langle \phi \rangle \neq 0$  breaks time reversal and splits the quadratic band touching point into four pairs of Weyl nodes along the [111] and symmetry-related axes in the cubic basis.

*Mean-field analysis.* We start by discussing the model on the level of mean-field theory at zero temperature. Formally, mean-field theory corresponds to the limit of large number  $N$  of quadratic band touching points at the Fermi level. This effectively suppresses fluctuations of the bosonic fields. The value of the order parameter is then obtained by minimizing the mean-field energy  $E_{\text{MF}}(\phi) = \frac{r}{2}\phi^2 + \sum_{i=1}^2 \int_{\vec{p}} \varepsilon_\phi^{(i)}(\vec{p})$ , where  $\varepsilon_\phi^{(1,2)}$  denote the two lower-branch

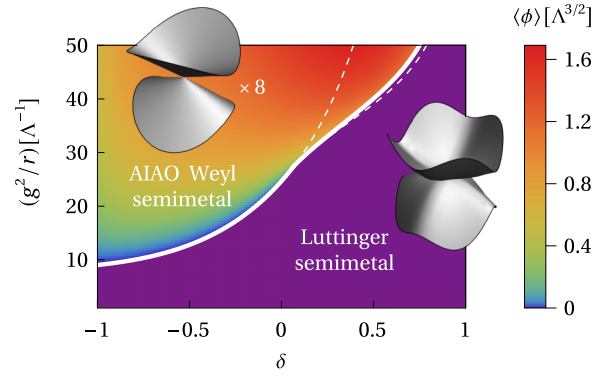


FIG. 2. Zero-temperature phase diagram of effective model as a function of cubic anisotropy  $\delta$  and interaction strength  $g^2/r$ , from mean-field theory. Coloring indicates the magnitude of the AIAO order parameter  $\langle \phi \rangle$ . With the onset of order, the quadratic band touching point of the Luttinger semimetal splits into four pairs of Weyl points in the AIAO Weyl semimetal (see insets). The transition is continuous (discontinuous) for  $\delta \leq \delta_0$  ( $\delta > \delta_0$ ), with  $\delta_0 \approx 0.0624$ . Dashed lines delimit the region in which metastable states exist.

eigenvalues of the mean-field Hamiltonian  $H_{\text{MF}} = \sum_{a=1}^5 (1 + s_a \delta) d_a(\vec{p}) \gamma_a + g\phi \gamma_{45}$  [see Supplemental Material (SM) (a) for details [36]]. The resulting phase diagram is presented in Fig. 2. We observe two distinct phases, the paramagnetic Luttinger semimetal phase and the time-reversal-broken Weyl semimetal phase. The former is located at small coupling below a finite threshold  $(g^2/r)_c$  and hosts a quadratic band touching point with fourfold degeneracy at zero momentum. The Weyl semimetal phase, characterized by a finite order parameter, is encountered above the phase boundary. It hosts four pairs of Weyl nodes along the [111] and symmetry-related axes in the electronic spectrum, and features AIAO order on the pyrochlore lattice. For anisotropies  $\delta \leq \delta_0 \approx 0.0624$ , we observe a continuous phase transition, while for  $\delta > \delta_0$ , the phase transition becomes discontinuous. The latter case gives rise to metastable states in the region around the transition, delimited by the dashed lines in Fig. 2. Importantly, *ab initio* calculations and photoemission spectroscopy experiments in  $\text{Pr}_2\text{Ir}_2\text{O}_7$  [9] suggest  $\delta < 0$ , placing this material into the regime with a continuous transition [37]. Note that at strong coupling, a second transition towards a Mott-insulating phase may be expected [21,23,38], which is not captured by the mean-field theory of our effective model. However, the presence or absence of this strong-coupling phase is irrelevant for the physics close to the quantum critical point between Luttinger and AIAO Weyl semimetals, which we will focus on in the following.

*Renormalization group analysis.* Note that the partially bosonized Lagrangian  $L = L_0 + L_a + L_\phi$  features a unique upper critical dimension, since both the Yukawa coupling  $g$  and the effective charge  $e$  become marginal in  $d = 4$  spatial dimensions. This allows a standard  $\epsilon = 4 - d$  expansion. We start by discussing the results at one-loop order, naively valid only for small  $\epsilon$ , but will then show that higher-loop corrections in fact vanish exactly at the AIAO Weyl quantum critical point. Integrating out modes with momenta  $q$  in the thin shell  $\Lambda/b < q < \Lambda$ , where  $\Lambda$  denotes the ultraviolet cutoff, and

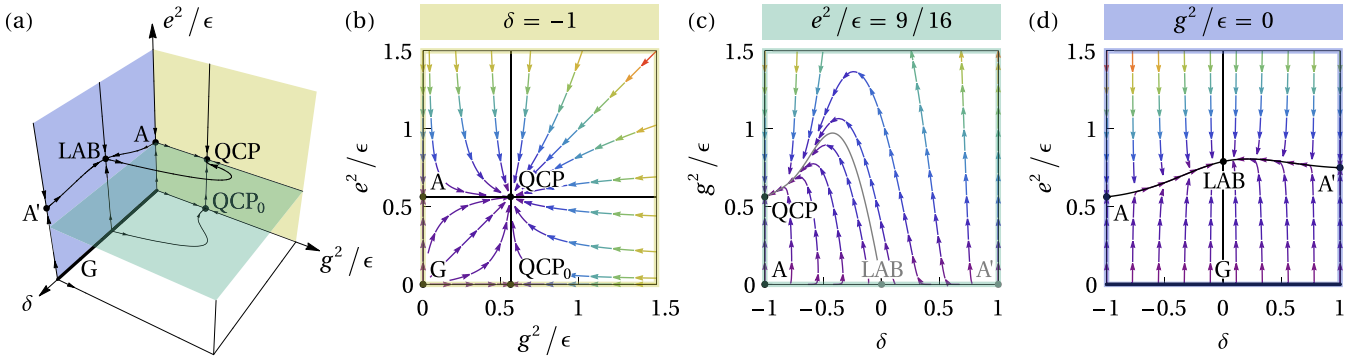


FIG. 3. Fixed-point structure for  $N = 1$  on the critical hypersurface  $r = 0$  in (a) the parameter space spanned by  $\delta$ ,  $g^2$ , and  $e^2$ , (b) the  $g^2$ - $e^2$  plane for fixed  $\delta = -1$ , (c) the  $\delta$ - $g^2$  plane for fixed  $e^2 = 9\epsilon/16$ , and (d) the  $\delta$ - $e^2$  plane for fixed  $g^2 = 0$ . Black (gray) dots and lines indicate fixed points and separatrices, respectively, located within (projected onto) the respective planes. Arrows denote flow towards the infrared, with their coloring indicating the flow velocity. There is a unique quantum critical fixed point at finite coupling, labeled as QCP. It corresponds to the continuous transition between the symmetric Luttinger semimetal and the AIAO-ordered Weyl semimetal. The symmetric state is described by the Luttinger-Abrikosov-Beneslavskii fixed point at  $g^2 = 0$ , labeled as LAB. The dots labeled as A, A', QCP<sub>0</sub>, and G correspond to unstable interacting and Gaussian, respectively, fixed points, further discussed in the SM.

arbitrary frequency, leads to the flow equations at criticality  $r = 0$  as [see SM (b) [36]]

$$\frac{d\delta}{d \ln b} = -\frac{2}{15}(1 - \delta^2)^2[(g^2 + e^2)f_{1e} + (g^2 - e^2)f_{1t}], \quad (4)$$

$$\begin{aligned} \frac{dg^2}{d \ln b} &= (\epsilon - \eta_\phi)g^2 - \frac{2}{15}(1 - \delta^2)[(1 + \delta)(g^2 + e^2)f_{1e} \\ &\quad - (1 - \delta)(g^2 - e^2)(f_{1t} - 3f_{2e})]g^2, \end{aligned} \quad (5)$$

$$\begin{aligned} \frac{de^2}{d \ln b} &= (\epsilon - \eta_a)e^2 - \frac{2}{15}(1 - \delta^2)[(1 + \delta)(g^2 + e^2)f_{1e} \\ &\quad - (1 - \delta)(g^2 - e^2)f_{1t}]e^2, \end{aligned} \quad (6)$$

where  $\eta_\phi = Ng^2f_g$  and  $\eta_a = Ne^2f_e$ . Here,  $f_i \equiv f_i(\delta)$  with  $i \in \{1e, 1t, 2e, e^2\}$  ( $i \in \{g^2\}$ ) are bounded and continuous functions of the anisotropy parameter  $\delta$  with  $f_i > 0$  ( $f_g \geq -2/3$ ) for  $\delta \in [-1, 1]$  and  $f_i = 1$  ( $f_g = 0$ ) for  $\delta = 0$ . Their definitions and numerical values for  $\delta \neq 0$  are given in SM (c) [36]. In the above flow equations, we have rescaled the couplings as  $(g^2, e^2)\Lambda^{-\epsilon}/(2\pi^2) \mapsto (1 - \delta^2)(g^2, e^2)$ , which turns out convenient to assess the properties of the stable fixed point. Note that this implies that higher-order loop corrections to the above equations will involve additional factors of  $(1 - \delta^2)$ . Importantly, in the present form, the stable fixed point associated with AIAO Weyl quantum criticality is located at finite couplings, as we show next.

Figure 3(a) depicts the fixed-point structure for  $N = 1$  on the critical hypersurface  $r = 0$  in the space spanned by the parameters  $\delta$ ,  $g^2$ , and  $e^2$ . Notably, both  $g^2$  and  $e^2$  are relevant couplings and flow towards a finite value in the infrared [Fig. 3(b)]. For finite  $g^2$ , the anisotropy parameter  $\delta$  then no longer has a fixed point at  $\delta = 0$ , and instead flows towards maximal anisotropy  $\delta = -1$  [Fig. 3(c)]. Most importantly, there is a unique stable fixed point at finite couplings, located at  $\delta_* = -1$  and  $g_*^2 = e_*^2 = 9\epsilon/(16N)$ . This fixed point, labeled as QCP in Figs. 3(a)–3(c), corresponds to the continuous quantum phase transition between the symmetric Luttinger semimetal, described by the Luttinger-Abrikosov-Beneslavskii fixed point [26–29] in the  $g = 0$  plane [Fig. 3(d)] and the AIAO-ordered Weyl semimetal. It is characterized

by finite boson anomalous dimensions  $\eta_\phi = \eta_a = \epsilon$ , vanishing fermion anomalous dimension  $\eta_\psi = 0$ , and a dynamical critical exponent  $z = 2$ . From the flow of the tuning parameter  $r$ , we furthermore obtain the correlation-length exponent  $\nu = 1/(2 - \epsilon)$ . In SM (d), we show that particle-hole symmetry becomes emergent at the quantum critical point [36]. SM (e) also contains a discussion of the other, unstable, fixed points [36].

The stable fixed point has remarkable properties. First of all, the fact that it is located at  $\delta_* = -1$  implies that higher-loop corrections to the vertex renormalizations [Eqs. (5) and (6)] vanish at criticality [see SM (f) for details [36]]. As a consequence, we find that our one-loop results  $z = 2$ ,  $\eta_\phi = \eta_a = 4 - d$ , and  $\nu = 1/(d - 2)$  hold at all loop orders at the quantum critical point. The transition between Luttinger and AIAO Weyl semimetals in the pyrochlore iridates therefore realizes a rare instance of an interacting fermionic quantum critical point in a three-dimensional system that allows an exact determination of its critical properties. With the exact results at hand, we can resolve an apparent contradiction in the literature concerning the relevance or irrelevance of the cubic anisotropy at this quantum critical point [24,25]. While the anisotropy parameter  $\delta$  vanishes at the Luttinger-Abrikosov-Beneslavskii fixed point, it flows towards  $\delta = -1$  at the quantum critical fixed point. Technically, the emergence of this maximal anisotropy at criticality arises from the order-parameter contributions to the fermion self-energy, which are neglected in the analysis of Ref. [25].

*Quasiuniversality.* In the vicinity of the quantum critical fixed point at  $\delta_* = -1$ , the flow of the anisotropy parameter takes the form

$$\left. \frac{d(\delta - \delta_*)}{d \ln b} \right|_{g_*^2, e_*^2} = -\frac{c\epsilon}{N}(\delta - \delta_*)^2 + O((\delta - \delta_*)^3), \quad (7)$$

with a constant  $c := 3f_{1e}(-1)/5 \approx 0.4449$ . Note the absence of a linear term  $\propto(\delta - \delta_*)$  in the above equation. The deviation  $(\delta - \delta_*)$  corresponds to a *marginally* irrelevant parameter, implying a logarithmically slow flow towards the critical point,  $\delta(b) - \delta_* \simeq N/(c\epsilon \ln b)$ , for  $\ln b \gg 1$ . By contrast, the Yukawa coupling and the effective charge acquire a power-law

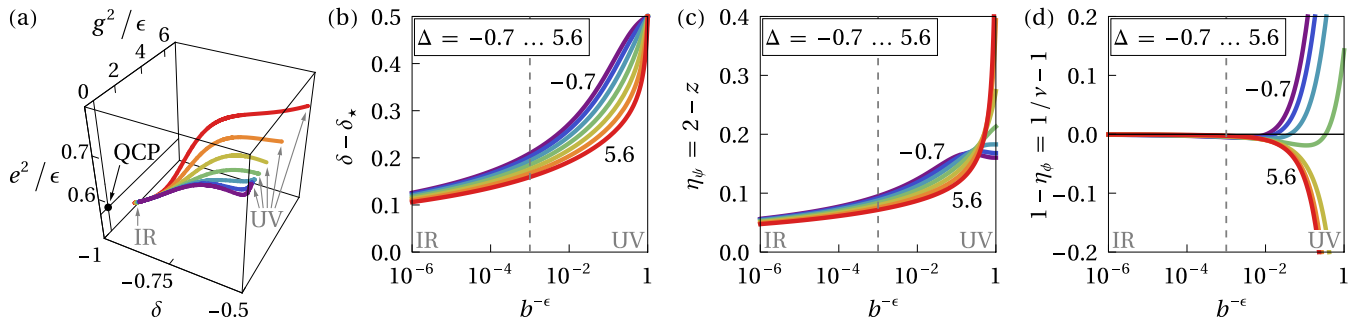


FIG. 4. Renormalization group flow on the critical hypersurface  $r = 0$  from the ultraviolet scale, corresponding to  $b^{-\epsilon} = 1$ , to a deep infrared scale, corresponding to  $b^{-\epsilon} = 10^{-6}$ , starting from different microscopic parameters. Each curve corresponds to a numerical integration of the flow equations using the initial conditions  $(\delta, g^2, e^2) = (-0.5, 0.7391, 0.9098 + \Delta)$  for  $b^{-\epsilon} = 1$ , with  $\Delta = -0.7, -0.6, -0.4, 0, 0.8, 2.4, 5.6$  from purple to red. The starting values of  $(g^2, e^2)$  have been chosen to satisfy the pseudo-fixed-point conditions for  $\delta = -0.5$  when  $\Delta = 0$ . (a) Flow trajectories in the parameter space spanned by  $\delta$ ,  $g^2$ , and  $e^2$ , illustrating the crossover from the nonuniversal regime, characterized by independent trajectories, to the quasiuniversal regime, in which these collapse onto a single curve. Deviations of (b) anisotropy parameter  $\delta$  and effective exponents (c)  $\eta_\psi = 2 - z$  and (d)  $\eta_\phi = 2 - 1/\nu$  from their respective critical values as a function of renormalization group scale  $b^{-\epsilon}$ . The quasiuniversal regime emerges at  $b^{-\epsilon} \lesssim 10^{-3}$ , as indicated by the dashed line, and manifests itself in  $(g^2, e^2)$ -independent, but anisotropy-dependent, drifting exponents. Note that the flow is still significantly away from its ultra-low-energy limit even at  $b^{-\epsilon} = 10^{-6}$ , as evidenced by the finite deviation  $\delta - \delta_* \gtrsim 0.1$  in (b).

flow,  $g^2(b) - g_*^2 \propto b^{-\epsilon}$  and  $e^2(b) - e_*^2 \propto b^{-\epsilon}$ . This implies a separation of scales, giving rise to the following three regimes in energy: In the nonuniversal high-energy regime, the couplings  $g^2$  and  $e^2$  flow from their microscopic values towards pseudo-fixed-point values  $g_*^2(\delta)$  and  $e_*^2(\delta)$ , which depend only on the anisotropy parameter  $\delta$ . Within this regime, the latter can be considered approximately constant. Its slow flow becomes visible only when several orders of magnitude in energy are considered. This defines a quasiuniversal intermediate-to-low-energy regime [2,6], in which the couplings  $g^2$  and  $e^2$  no longer depend on their microscopic values, but solely follow their pseudo-fixed-point values  $g_*^2(\delta)$  and  $e_*^2(\delta)$  with a slowly varying anisotropy parameter  $\delta$ . In this regime, the correlation length becomes large, such that observables display approximate power laws with slowly drifting exponents [39,40]. Finally, the genuinely universal ultra-low-energy regime will be reached only after the anisotropy parameter has approached its ultimate infrared regime, which requires fluctuations on unusually many energy scales to be integrated out.

This is exemplified in Fig. 4, which shows the numerically integrated renormalization group flow for different initial couplings on the critical hypersurface  $r = 0$ . The couplings  $g^2$  and  $e^2$  first exhibit a fast flow on individual, nonuniversal trajectories, but then approach a single, quasiuniversal trajectory of pseudo-fixed points  $(g_*^2(\delta), e_*^2(\delta))$ , along which they only slowly flow, as a consequence of the slow flow of  $\delta$  [Fig. 4(a)]. In fact, even after six orders of magnitude in  $b^\epsilon$  have been integrated out,  $\delta$  is still significantly away from its ultra-low-energy value  $\delta_* = -1$  [Fig. 4(b)]. There is therefore a large quasiuniversal regime characterized by approximate power laws with effective critical exponents, which are only slowly drifting with energy or length. As shown in SM (b) [36], the present model satisfies additional scaling relations between the different exponent, viz.,  $z = 2 - \eta_\psi$  and  $1/\nu = 2 - \eta_\phi$ . There are therefore only two independent effective exponents. Their slow drifts as a function of scale are depicted in Figs. 4(c) and 4(d), illustrating the fact that the

genuinely universal values are reached, at least for some of the exponents, only in the ultra-low-energy limit. We emphasize that the slow renormalization group flow is independent of microscopic parameters and as such will occur in any given material realization of the AIAO Weyl quantum critical point in Luttinger semimetals. In SM (g) [36], we compare the quasiuniversal flow with a generic power-law flow of a toy model that does not feature a marginal coupling, illustrating the unusual behavior observed in the quasiuniversal regime.

*Experiments.* The quasiuniversal regime is separated by crossovers from the nonuniversal regime at the ultraviolet scale and the genuinely universal regime in the deep infrared, and realizes a novel strongly interacting quantum state of matter. For the pyrochlore iridates, the relevant energy scale above which the physics depends on microscopic details of the material is around 100 K [18]. Assuming  $z \simeq 2$ , each order of magnitude in energy corresponds to only half an order of magnitude in  $b^\epsilon$ , if  $\epsilon = 1$ . The ultra-low-temperature behavior will therefore be reached only well below the 1 mK regime. Such a regime is not only difficult to access experimentally and necessitates sufficiently pure crystals that do not cut off the required long-range fluctuations: In the case of the pyrochlore iridates, we also expect new effects in this ultra-low-energy regime, arising from the weak Kondo coupling of the iridium electrons to the rare-earth local moments [41,42]. The experimentally most easily accessible regime below 100 K, by contrast, will be governed by quasiuniversal behavior, characterized by approximate power laws with slowly drifting exponents. The specific heat as a function of temperature, for instance, is expected to scale as  $C \sim T^{d/z}$  with drifting exponent  $d/z > 3/2$  at around 100 K and  $d/z = 3/2$  in the ultra-low-temperature limit. Observing such drifting exponents, e.g., in careful thermodynamic and/or transport measurements, would accomplish the experimental realization of this state of matter.

*Conclusions.* We have demonstrated the emergence of a quasiuniversal regime, which should be understood as a differ-

ent strongly interacting quantum state of matter, in the finite-temperature phase diagram of interacting three-dimensional Luttinger semimetals. While quasiuniversal behavior is usually associated with a fixed-point annihilation scenario [2,3], our results show that the presence of a marginally irrelevant operator can lead to the same phenomenology. Our findings call for experiments on sufficiently pure samples of pyrochlore iridates  $R_2\text{Ir}_2\text{O}_7$ , which search for power laws with slowly drifting exponents in the intermediate-energy regime above the Weyl-Luttinger quantum phase transition [20,43]. In the ultra-low-energy regime, by contrast, the weak Kondo coupling between the iridium electrons and the rare-earth

local moments might lead to even more intriguing effects, the study of which represents an excellent direction for future theoretical work.

*Acknowledgments.* We thank Igor Boettcher, Santanu Dey, Igor Herbut, and Joseph Maciejko for illuminating discussions, and Igor Boettcher and Igor Herbut for helpful comments on the manuscript. This work has been supported by the Deutsche Forschungsgemeinschaft (DFG) through SFB 1143 (A07, Project No. 247310070), the Würzburg-Dresden Cluster of Excellence ct.qmat (EXC 2147, Project No. 390858490), and the Emmy Noether program (JA2306/4-1, Project No. 411750675).

- 
- [1] C. Wang, A. Nahum, M. A. Metlitski, C. Xu, and T. Senthil, Deconfined quantum critical points: Symmetries and dualities, *Phys. Rev. X* **7**, 031051 (2017).
- [2] A. Nahum, Note on Wess-Zumino-Witten models and quasiuniversality in  $2 + 1$  dimensions, *Phys. Rev. B* **102**, 201116(R) (2020).
- [3] R. Ma and C. Wang, Theory of deconfined pseudocriticality, *Phys. Rev. B* **102**, 020407(R) (2020).
- [4] T. Senthil, A. Vishwanath, L. Balents, S. Sachdev, and M. P. A. Fisher, Deconfined quantum critical points, *Science* **303**, 1490 (2004).
- [5] T. Senthil, L. Balents, S. Sachdev, A. Vishwanath, and M. P. A. Fisher, Quantum criticality beyond the Landau-Ginzburg-Wilson paradigm, *Phys. Rev. B* **70**, 144407 (2004).
- [6] A. Nahum, J. T. Chalker, P. Serna, M. Ortuño, and A. M. Somoza, Deconfined quantum criticality, scaling violations, and classical loop models, *Phys. Rev. X* **5**, 041048 (2015).
- [7] B. Irgig, N. Zerf, P. Marquard, I. F. Herbut, and M. M. Scherer, Abelian Higgs model at four loops, fixed-point collision, and deconfined criticality, *Phys. Rev. B* **100**, 134507 (2019).
- [8] H. Shao, W. Guo, and A. W. Sandvik, Quantum criticality with two length scales, *Science* **352**, 213 (2016).
- [9] T. Kondo, M. Nakayama, R. Chen, J. J. Ishikawa, E. G. Moon, T. Yamamoto, Y. Ota, W. Malaeb, H. Kanai, Y. Nakashima, Y. Ishida, R. Yoshida, H. Yamamoto, M. Matsunami, S. Kimura, N. Inami, K. Ono, H. Kumigashira, S. Nakatsuji, L. Balents *et al.*, Quadratic Fermi node in a 3D strongly correlated semimetal, *Nat. Commun.* **6**, 10042 (2015).
- [10] M. Nakayama, T. Kondo, Z. Tian, J. J. Ishikawa, M. Halim, C. Bareille, W. Malaeb, K. Kuroda, T. Tomita, S. Ideta, K. Tanaka, M. Matsunami, S. Kimura, N. Inami, K. Ono, H. Kumigashira, L. Balents, S. Nakatsuji, and S. Shin, Slater to Mott crossover in the metal to insulator transition of  $\text{Nd}_2\text{Ir}_2\text{O}_7$ , *Phys. Rev. Lett.* **117**, 056403 (2016).
- [11] N. P. Armitage, E. J. Mele, and A. Vishwanath, Weyl and Dirac semimetals in three-dimensional solids, *Rev. Mod. Phys.* **90**, 015001 (2018).
- [12] B. Q. Lv, T. Qian, and H. Ding, Experimental perspective on three-dimensional topological semimetals, *Rev. Mod. Phys.* **93**, 025002 (2021).
- [13] C. Brüne, C. X. Liu, E. G. Novik, E. M. Hankiewicz, H. Buhmann, Y. L. Chen, X. L. Qi, Z. X. Shen, S. C. Zhang, and L. W. Molenkamp, Quantum Hall effect from the topological surface states of strained bulk HgTe, *Phys. Rev. Lett.* **106**, 126803 (2011).
- [14] A. Barfuss, L. Dudy, M. R. Scholz, H. Roth, P. Höpfner, C. Blumenstein, G. Landolt, J. H. Dil, N. C. Plumb, M. Radovic, A. Bostwick, E. Rotenberg, A. Fleszar, G. Bihlmayer, D. Wortmann, G. Li, W. Hanke, R. Claessen, and J. Schäfer, Elemental topological insulator with tunable Fermi level: Strained  $\alpha$ -Sn on InSb(001), *Phys. Rev. Lett.* **111**, 157205 (2013).
- [15] B. Cheng, T. Ohtsuki, D. Chaudhuri, S. Nakatsuji, M. Lippmaa, and N. P. Armitage, Dielectric anomalies and interactions in the three-dimensional quadratic band touching Luttinger semimetal  $\text{Pr}_2\text{Ir}_2\text{O}_7$ , *Nat. Commun.* **8**, 2097 (2017).
- [16] K. Wang, B. Xu, C. W. Rischau, N. Bachar, B. Michon, J. Teyssier, Y. Qiu, T. Ohtsuki, B. Cheng, N. P. Armitage, S. Nakatsuji, and D. van der Marel, Unconventional free charge in the correlated semimetal  $\text{Nd}_2\text{Ir}_2\text{O}_7$ , *Nat. Phys.* **16**, 1194 (2020).
- [17] E. Y. Ma, Y.-T. Cui, K. Ueda, S. Tang, K. Chen, N. Tamura, P. M. Wu, J. Fujioka, Y. Tokura, and Z.-X. Shen, Mobile metallic domain walls in an all-in-all-out magnetic insulator, *Science* **350**, 538 (2015).
- [18] W. Witczak-Krempa, G. Chen, Y. B. Kim, and L. Balents, Correlated quantum phenomena in the strong spin-orbit regime, *Annu. Rev. Condens. Matter Phys.* **5**, 57 (2014).
- [19] S. Nakatsuji, Y. Machida, Y. Maeno, T. Tayama, T. Sakakibara, J. van Duijn, L. Balicas, J. N. Millican, R. T. Macaluso, and J. Y. Chan, Metallic spin-liquid behavior of the geometrically frustrated Kondo lattice  $\text{Pr}_2\text{Ir}_2\text{O}_7$ , *Phys. Rev. Lett.* **96**, 087204 (2006).
- [20] K. Ueda, T. Oh, B.-J. Yang, R. Kaneko, J. Fujioka, N. Nagaosa, and Y. Tokura, Magnetic-field induced multiple topological phases in pyrochlore iridates with Mott criticality, *Nat. Commun.* **8**, 15515 (2017).
- [21] W. Witczak-Krempa and Y. B. Kim, Topological and magnetic phases of interacting electrons in the pyrochlore iridates, *Phys. Rev. B* **85**, 045124 (2012).
- [22] W. Witczak-Krempa, A. Go, and Y. B. Kim, Pyrochlore electrons under pressure, heat, and field: Shedding light on the iridates, *Phys. Rev. B* **87**, 155101 (2013).
- [23] C. Berke, P. Michetti, and C. Timm, Stability of the Weyl-semimetal phase on the pyrochlore lattice, *New J. Phys.* **20**, 043057 (2018).
- [24] L. Savary, E.-G. Moon, and L. Balents, New type of quantum criticality in the pyrochlore iridates, *Phys. Rev. X* **4**, 041027 (2014).

- [25] I. Boettcher and I. F. Herbut, Anisotropy induces non-Fermi-liquid behavior and nematic magnetic order in three-dimensional Luttinger semimetals, *Phys. Rev. B* **95**, 075149 (2017).
- [26] A. A. Abrikosov and S. D. Beneslavskii, Possible existence of substances intermediate between metals and dielectrics, *Zh. Eksp. Teor. Fiz.* **59**, 1280 (1970) [*Sov. Phys. JETP* **32**, 699 (1971)].
- [27] A. A. Abrikosov, Calculation of critical indices for zero-gap semiconductors, *Zh. Eksp. Teor. Fiz.* **66**, 1443 (1974) [*Sov. Phys. JETP* **39**, 709 (1974)].
- [28] E.-G. Moon, C. Xu, Y. B. Kim, and L. Balents, Non-Fermi-liquid and topological states with strong spin-orbit coupling, *Phys. Rev. Lett.* **111**, 206401 (2013).
- [29] I. F. Herbut and L. Janssen, Topological Mott insulator in three-dimensional systems with quadratic band touching, *Phys. Rev. Lett.* **113**, 106401 (2014).
- [30] L. Janssen and I. F. Herbut, Nematic quantum criticality in three-dimensional Fermi system with quadratic band touching, *Phys. Rev. B* **92**, 045117 (2015).
- [31] S. Murakami, N. Nagaosa, and S.-C. Zhang, SU(2) non-Abelian holonomy and dissipationless spin current in semiconductors, *Phys. Rev. B* **69**, 235206 (2004).
- [32] J. M. Luttinger, Quantum theory of cyclotron resonance in semiconductors: General theory, *Phys. Rev.* **102**, 1030 (1956).
- [33] L. Janssen and I. F. Herbut, Excitonic instability of three-dimensional gapless semiconductors: Large- $N$  theory, *Phys. Rev. B* **93**, 165109 (2016).
- [34] L. Janssen and I. F. Herbut, Phase diagram of electronic systems with quadratic Fermi nodes in  $2 < d < 4$ :  $2 + \epsilon$  expansion,  $4 - \epsilon$  expansion, and functional renormalization group, *Phys. Rev. B* **95**, 075101 (2017).
- [35] K. Ladovrechis, T. Meng, and B. Roy, Competing magnetic orders and multipolar Weyl fermions in 227 pyrochlore iridates, *Phys. Rev. B* **103**, L241116 (2021).
- [36] See Supplemental Material at <http://link.aps.org/supplemental/10.1103/PhysRevB.109.L081111> for (a) technical details of the mean-field analysis, (b) the derivation of the flow equations, (c) definitions and numerical values of the solid-angle integrals, (d) a discussion of emergent particle-hole symmetry at the quantum critical point, (e) a review of the unstable fixed points, (f) an investigation of higher-loop corrections, and (g) a comparison of the quasiuniversal flow with a generic flow, which includes Ref. [44,45].
- [37] The hopping parameters in the lattice model of Ref. [22] indicate  $\delta \approx -0.07$ , which is qualitatively consistent with the Tran-Blaha modified Becke-Johnson (TB-mBJ) calculations of Ref. [9]. We thank I. Boettcher for helpful communication on this point.
- [38] X. Wan, A. M. Turner, A. Vishwanath, and S. Y. Savrasov, Topological semimetal and Fermi-arc surface states in the electronic structure of pyrochlore iridates, *Phys. Rev. B* **83**, 205101 (2011).
- [39] J. Schwab, L. Janssen, K. Sun, Z. Y. Meng, I. F. Herbut, M. Vojta, and F. F. Assaad, Nematic quantum criticality in Dirac systems, *Phys. Rev. Lett.* **128**, 157203 (2022).
- [40] E. J. Dresselhaus, B. Sbierski, and I. A. Gruzberg, Numerical evidence for marginal scaling at the integer quantum Hall transition, *Ann. Phys. (NY)* **435**, 168676 (2021).
- [41] X.-P. Yao and G. Chen, Pr<sub>2</sub>Ir<sub>2</sub>O<sub>7</sub>: When Luttinger semimetal meets Melko-Hertog-Gingras spin ice state, *Phys. Rev. X* **8**, 041039 (2018).
- [42] K. Ueda, H. Ishizuka, M. Kriener, S. Kitou, D. Maryenko, M. Kawamura, T.-H. Arima, M. Kawasaki, and Y. Tokura, Experimental signatures of a versatile Weyl semimetal in a pyrochlore iridate with spin-ice-like magnetic orders, *Phys. Rev. B* **105**, L161102 (2022).
- [43] P. Nikolić, Y. Xu, T. Ohtsuki, S. Nakatsuji, and N. Driehko, Weyl-Luttinger phase transition in pyrochlore iridates revealed by Raman scattering, [arXiv:2204.13722](https://arxiv.org/abs/2204.13722).
- [44] S. Ray and L. Janssen, Gross-Neveu-Heisenberg criticality from competing nematic and antiferromagnetic orders in bilayer graphene, *Phys. Rev. B* **104**, 045101 (2021).
- [45] M. Vojta, Y. Zhang, and S. Sachdev, Renormalization group analysis of quantum critical points in  $d$ -wave superconductors, *Int. J. Mod. Phys. B* **14**, 3719 (2000).